Eur. Phys. J. D **33**, 29–33 (2005)
DOI: 10.1140/epjd/e2005-00022-0

THE EUROPEAN PHYSICAL JOURNAL D

Pressure broadening parameters of the hydroxyl radical A $^2\Sigma^+$ ($v' = 0$) ← X $^2\Pi_{3/2}$ ($v'' = 0$) transitions at ca. 308 nm*

V.L. Kasyutich[a]

School of Chemical Engineering and Analytical Science, University of Manchester, P.O. Box 88, Manchester, M60 1QD, UK

Received 3 November 2004 / Received in final form 21 December 2004
Published online 8 February 2005 –

Abstract. Pressure broadening widths and pressure-induced frequency shifts for the hydroxyl radical $Q_{11}(1)$, $Q_{21}(1)$, $Q_{11}(2)$, $Q_{21}(2)$ absorption lines in the A $^2\Sigma^+$ ($v' = 0$) ← X $^2\Pi_{3/2}$ ($v'' = 0$) band at ca. 308 nm have been determined in the presence of a variety of gases (N_2, Ar, Ne and He). Hydroxyl radicals were formed using either a microwave discharge or a vacuum ultra-violet photolysis of water vapour and were detected using direct absorption spectroscopy with a bandwidth normalised noise equivalent absorption sensitivity of 5×10^{-5} $Hz^{-1/2}$. A tunable external cavity diode laser at 835 nm and a single-frequency continuous-wave intracavity frequency-doubled diode laser at 488 nm were used to produce tunable continuous-wave light at 308 nm by sum-frequency generation in a $\beta-BaB_2O_4$ crystal.

PACS. 33.70.Jg Line and band widths, shapes, and shifts – 33.20.Lg Ultraviolet spectra – 42.55.Px Semiconductor lasers; laser diodes – 42.65.Ky Frequency conversion; harmonic generation, including higher-order harmonic generation

1 Introduction

Tunable ultra-violet (UV) continuous-wave (cw) sources based on frequency doubling and sum-frequency generation with laser diodes have been widely used in detection of many species with strong electronic transitions in the UV spectral region (200–400 nm) [1–4]. These transitions are typically one or two orders of magnitude stronger than the mid-infrared transitions. For instance, the hydroxyl radical (OH), which is one of the most important species in atmospheric chemistry [4], has a maximum effective absorption cross-section of $\sim 2 \times 10^{-16}$ cm^2 $molecule^{-1}$ near 308 nm at ∼300 K and atmospheric pressure [5]. Broadening of OH absorption lines induced by collisions with nitrogen, oxygen, inert gases and water is of interest [6], since it is involved in many experimental measurements. However, fewer measurements for ground-state OH X $^2\Pi$ broadening parameters have been reported [5,7,8]. Moreover, there are discrepancies for the OH broadening widths by He and Ne in [7,8] and the OH pressure broadening widths by N_2, O_2 and Ar determined in [7,8] are consistently lower than ones published in [5].

In this paper we demonstrate the use of a tunable narrow band UV source based on sum-frequency generation with an external cavity diode laser at 835 nm and a stable single-frequency continuous-wave intracavity frequency-doubled diode laser at 488 nm. Measurements of pressure broadening width and pressure-induced shift of the $Q_{11}(1)$, $Q_{21}(1)$, $Q_{11}(2)$, $Q_{21}(2)$ OH absorption lines for N_2, Ar, Ne and He have been performed. An empirical Parmenter-Seaver relationship was used to analyse experimental pressure broadening widths and to determine the OH pressure broadening width by O_2.

2 Experimental

The experimental set-up used in the OH pressure broadening studies is shown in Figure 1. An infra-red (IR) diode laser (Sacher Lasertechnik Littrow laser TEC100-835-100) was tuned mode-hop free around 835 nm within a range of 40–60 GHz. The collimated IR beam passed through an anamorphic prism pair (PS-871-B, Thorlabs), a broadband optical isolator (Isowave I-7090-CM, isolation >40 dB) and a half-wave plate to control the polarisation of the light. The IR laser optical spectrum and frequency scan range were monitored using a commercial optical spectrum analyser (Melles Griot, free spectral range of 2 GHz). The output signal of the spectrum analyser was used for frequency calibration of the spectra. A single-frequency cw intracavity frequency-doubled diode laser (Protera-488, Novalux) was used as a 488 nm light source. According to manufacturers the laser line widths had quoted bandwidths of less than 18 MHz and 10 MHz at 488 nm and 835 nm, respectively. The laser

* The work was performed at the Physical and Theoretical Chemistry Laboratory, University of Oxford, UK.

[a] e-mail: Vasili.Kasiutsich@manchester.ac.uk

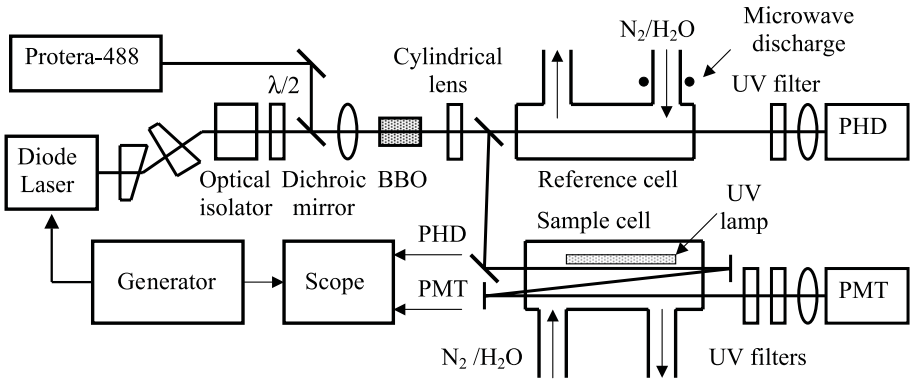

Fig. 1. Experimental set-up: BBO is a β–BaB_2O_4 crystal; PHD is a photodiode; PMT is a photomultiplier tube.

wavelenghts were monitored by means of a wavelength meter (Wavemaster, Coherent Inc.).

The vertically polarised 835 nm and 488 nm beams were combined by means of a dichroic mirror and focused into a $\beta-BaB_2O_4$ crystal ($4 \times 4 \times 10$ mm^3, CASTECH) cut for type I phase matching. The UV beam was then directed by means of a mirror in a flipper mount either into a reference cell at low pressure or a sample cell at atmospheric pressure. The UV power was measured using a photodiode (S1336-5BQ, Hamamatsu). We calculate a theoretical conversion efficiency of $\gamma_{\rm th} = 6.75 \times 10^{-4}$ W^{-1} for a lossless crystal [9], while our experimental conversion efficiency was estimated as $\gamma_{\rm exp} = (4 \pm 0.4) \times 10^{-4}$ W^{-1} with a maximum UV output of 170±17 nW obtained from experiments with the 835 nm and 488 nm laser beam powers of 26 mW and 16 mW, respectively. Power conversion efficiency was calculated to be 4.05×10^{-4}%.

The reference cell was a Pyrex tube (inner diameter of 3.5 cm, length of 70 cm) fitted with wedge fused quartz windows. OH radicals were produced in the reference cell by using a 2.45 GHz microwave discharge in an N_2/H_2O mixture at pressure of 0.3 Torr. The UV beam passed through the middle of the reference cell and a filter (UG11) and then was focused onto a photodiode (S1337-5BQ, Hamamatsu). The photodiode signal was amplified with an equivalent noise bandwidth of 5.32 kHz and recorded with a digital oscilloscope (Lecroy 9304).

The sample cell was a Pyrex tube (inner diameter of 3.5 cm, length of 50 cm) fitted with wedge fused quartz windows. A mercury Pen-Ray lamp (3SC-9, Ultra-Violet Products Ltd), with illuminated length of ∼23 cm, was inserted within the sample cell. Nitrogen, argon, neon and helium (BOC Gases) were bubbled through distilled water before passing through the sample cell at atmospheric pressure of 760 ± 10 Torr. OH radicals were generated inside the sample cell by vacuum UV photolysis of water vapour. The temperature inside the cell was 300±1 K, while the ambient temperature was 294±1 K. Water vapour concentrations were estimated by direct absorption at 1320.126 nm (vacuum wavelength) of radiation from a distributed feedback diode laser (Marconi Caswell Ltd). The UV beam passed through the cell three times (a total optical path of 1.5 m), an interference filter (transmittance of 30% at 308 nm) and an optical filter (UG11) and was then focused onto a photomultiplier tube (PMT) (QL30F/RFI, Thorn EMI) loaded by a 100 K resistor. The PMT output was connected directly to an oscilloscope terminated with a 1 MΩ input impedance, to give an equivalent noise bandwidth of 7.86 kHz. A ramp modulation waveform at a frequency of 11 Hz was applied on the IR diode laser driver to tune the IR diode laser wavelength and hence to tune the UV light wavelength across the A $^2\Sigma^+$ ($\upsilon' = 0$) ← X $^2\Pi_{3/2}$ ($\upsilon'' = 0$) OH absorption transitions.

3 Results

Direct absorption spectra of the $Q_{11}(1)$ + $Q_{21}(1)$ and $Q_{11}(2)$ + $Q_{21}(2)$ pair lines of OH are shown in Figure 2a (nitrogen in the sample cell) and Figure 2b (argon in the sample cell), respectively. The absorption spectra were computed according to the Beer-Lambert law as $\ln(I_{\rm off}/\ I_{\rm on})$, where $I_{\rm on}$ and $I_{\rm off}$ were the signals from the photodetectors recorded with OH radicals inside the cells and without OH radicals inside the cell, i.e. when the vacuum UV lamp or the microwave discharge were switched on and then off. To ensure that there was no significant drift in the UV frequency, the absorption OH spectra from the reference cell were recorded before and after the recording the signals from the sample cell and were then compared.

From the OH spectra recorded at low pressure (Figs. 2a and 2b) and fitted with Gaussian functions, an average line full width at half maximum (FWHM) was estimated to be 2.9 ± 0.09 GHz. This value was equal within experimental errors to the Doppler broadening OH linewidth of 2.9 GHz calculated at a temperature of 294 K. Thus, we assumed that effect of the UV light linewidth on the OH line broadening was negligible in the pressure broadening measurements. All spectra recorded at atmospheric pressure were fitted to a Voigt profile. Best fits were obtained when the Gaussian component was constrained to the width of 2.929 GHz that was equal to the OH Doppler width at a temperature of 300 K. The fitting program (Microcal $^{\rm TM}$Origin, v. 6.0) returned the Lorentzian component and the peak relative frequency position that was used in the calculation of pressure-induced frequency

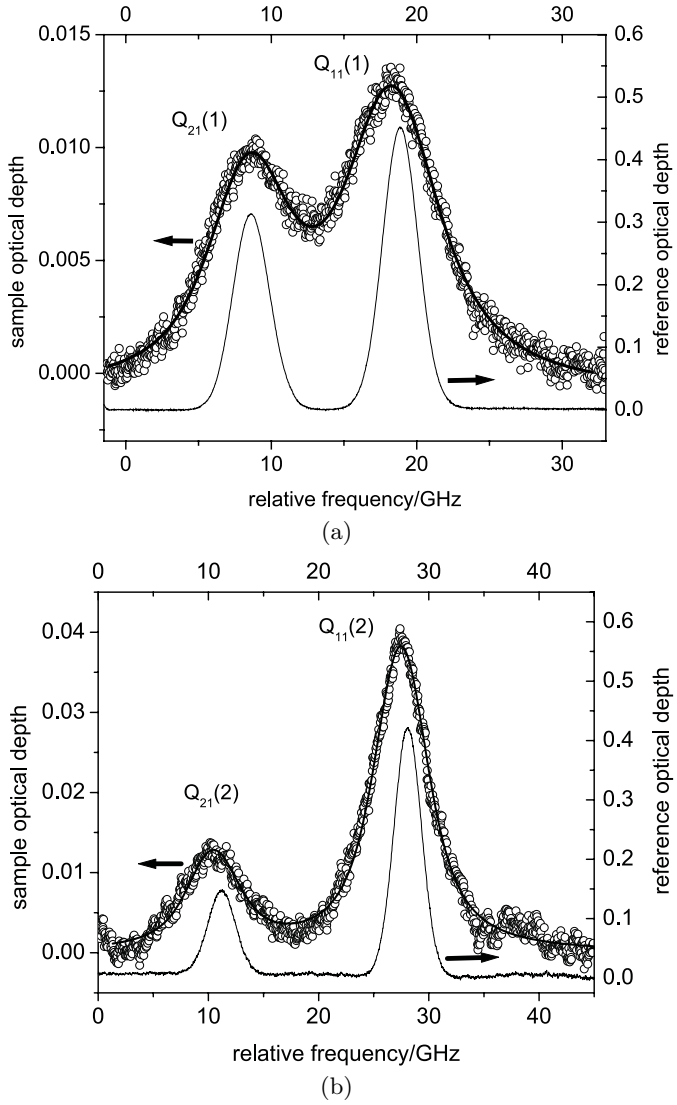

Fig. 2. Absorption spectra of the $Q_{11}(1)$ + $Q_{21}(1)$ line pair in nitrogen (a) and $Q_{11}(2)$ + $Q_{21}(2)$ line pair in argon (b) at an IR diode laser scan frequency of 11 Hz, an average of 100 sweeps: circles – experimental spectra recorded in the sample cell at 300 K and atmospheric pressure; line – the Voigt fit to two lines; narrow peaks line – the experimental spectra recorded in the reference cell at pressure of 0.3 Torr.

shift. Bandwidth normalised noise equivalent absorptions of 6×10^{-5} $Hz^{-1/2}$ and 5×10^{-5} $Hz^{-1/2}$ were estimated from the absorption spectra in Figure 2 recorded at low and atmospheric pressures, respectively.

For the spectra in Figure 2a the peak absorption cross-section was estimated to be 4.9×10^{-16} cm^2 $molecule^{-1}$ and 1.5×10^{-16} cm^2 $molecule^{-1}$ for $Q_{11}(1)$ OH line absorption in the reference cell at low pressure and in the sample cell at atmospheric pressure, respectively. For the spectra in Figure 2b the peak absorption cross-section was estimated to be 6.2×10^{-16} cm^2 $molecule^{-1}$ and 2.5×10^{-16} cm^2 $molecule^{-1}$ for $Q_{11}(2)$ OH line absorption in the reference cell at low pressure and in the sample cell at atmospheric pressure, respectively. The Einstein coefficients, the OH relative population densities and the line-centre wavenumbers were taken from the LIFBASE [10]. It was assumed that the Doppler line shape factor was 1.06 [5], and the Voigt line shape factors of 1.48 (nitrogen in the sample cell) and 1.42 (argon in the sample cell) were calculated according to Whiting [11]. From the spectra in Figure 2 the hydroxyl radical concentrations were estimated to be in the range of $1-1.3 \times 10^{13}$ molecule cm^{-3} and $0.4-1.1 \times 10^{12}$ molecule cm^{-3} in the reference cell and the sample cell, respectively.

The lineshape at atmospheric pressure results from the Doppler broadening and collisional broadening by the buffer gas and water. We measured a partial pressure of ∼12 Torr H_2O by means of diode laser absorption at 1.32 μm, somewhat lower than the saturated vapour pressure at 294 K of 18.65 Torr. We estimated, using data from references [7,9], that the water vapour contributed approximately 200 MHz to the OH collisional full linewidth at atmospheric pressure. In our measurements of the OH pressure-induced line shifts we assumed that the OH line pressure shifts induced by H_2O were negligible.

Table 1 shows the purely collisional broadening widths (FWHM) and pressure-induced frequency shifts measured in the presence of N_2, Ar, Ne and He along with the Boltzmann average over the probed quantum states. Experimental data from the references [7,8] are also shown. Errors indicate one standard deviation of ten measurements for each gas. Data errors in the measured collisional widths and shifts appear dominantly from statistical errors in the frequency scale (the scale was determined from the 2 GHz etalon) and statistical errors of the Lorentzian component in the Voigt fitting because of the moderate signal/noise ratios in spectra recorded at atmospheric pressure.

4 Discussion

We first note the OH pressure broadening widths shown in Table 1. Although the present values apply strictly only to the specific transitions, qualitative comparisons with other transitions probing similar quantum numbers are valid. This is because the broadening depends largely upon the relative energy of the eigenstates of the isolated species and on the potential between colliding partners. Our measured magnitudes of the pressure broadening widths are comparable, within experimental errors, with previous experimental data determined for the $P_{11}(2)$ line [8] and the average of different UV lines of the A $^2\Sigma^+$ ($v' = 0$) ← X $^2\Pi_{3/2}$ ($v'' = 0$) band at ca. 308 nm [7]. We note that our present measured pressure broadening widths of the $Q_{11}(2)$ and $Q_{21}(2)$ transitions are found to be smaller (1.3 GHz in case of Ne and 0.8 GHz in case of He) than estimated from UV cavity enhanced absorption experiments at atmospheric pressure [9], and we explain this discrepancy as being due to the contribution of the OH radicals, whose transitions were broadened by atmospheric air in open parts of the cavity.

Table 1. Pressure broadening widths and pressure-induced frequency shifts for the four absorption OH lines with four collision partners at temperature of 300 K. For comparison also shown are an average collisional width of A $^2\Sigma^+$ ($\upsilon' = 0$) $\leftarrow$ X $^2\Pi$ ($\upsilon'' = 0$) lines measured at temperature of 293 [7] and collisional parameters for $P_{11}(2)$ line measured at temperature of 296 K [8]. Errors indicate one standard deviation of ten measurements for each gas.

	N_2	N_2	Ar	Ar	Ne	Ne	He	He
Transition	Width/ GHz atm^{-1}	Shift/ GHz atm^{-1}	Width/ GHz atm^{-1}	Shift/ GHz atm^{-1}	Width/ GHz atm^{-1}	Shift/ GHz atm^{-1}	Width/ GHz atm^{-1}	Shift/ GHz atm^{-1}
$Q_{11}(1)$	5.7 ± 0.8	–0.6 ± 0.1	3.5 ± 0.3	–0.67 ± 0.08	2.2 ± 0.2	–0.34 ± 0.02	2.6 ± 0.5	–0.3 ± 0.1
$Q_{21}(1)$	5.5 ± 0.6	–0.3 ± 0.1	3.8 ± 0.2	–0.5 ± 0.05	2.4 ± 0.4	–0.19 ± 0.05	2.0 ± 0.7	–0.3 ± 0.1
$Q_{11}(2)$	5.3 ± 0.8	–0.4 ± 0.1	3.8 ± 0.4	–0.6 ± 0.1	1.8 ± 0.3	–0.66 ± 0.1	1.7 ± 0.2	–0.3 ± 0.1
$Q_{21}(2)$	4.6 ± 1.0	–0.5 ± 0.1	3.3 ± 1.2	–0.6 ± 0.2	2.4 ± 1.1	–0.65 ± 0.3	2.3 ± 1.4	–0.5 ± 0.3
Boltzmann weighted average	5.3 ± 0.8	–0.45 ± 0.1	3.6 ± 0.5	–0.6 ± 0.1	2.2 ± 0.5	–0.46 ± 0.1	2.1 ± 0.8	–0.3 ± 0.2
Average [7]	4.3		4.0 ± 0.4		1.9		1.5	
$P_{11}(2)$ [8]	6.5 ± 0.16	–0.44 ± 0.05	4.2 ± 0.07	–0.92 ± 0.01	1.46 ± 0.16	–0.44 ± 0.05	1.71 ± 0.07	–0.3 ± 0.01

The collision cross section for OH A $^2\Sigma^+$ ($\upsilon' = 0$) transitions do not correlate well with parameters such as polarisability and molecular radius, which are indicative of dispersion forces between OH and the collision partner [12]. The empirical Parmenter-Seaver (PS) well-depth correlation [13] was used to analyse and predict the collision cross sections of OH (A $^2\Sigma^+$ ($\upsilon' = 0$) state) and the collision partner at 200 K with reasonable accuracy, except for N_2 [12]. The PS well-depth model proposes that attractive forces dominate the collision broadening process. According to the PS model for collision process between species A (e.g. hydroxyl) and a variety of colliding partners, M, the collision cross section σ is expected to follow the relationship [13]

$$\ln \sigma = C + B\sqrt{\varepsilon_{\mathrm{MM}}/k} \qquad (1)$$

where C, B are constants, $\varepsilon_{\mathrm{MM}}$ is the potential well depth of the dimer M_2, k is the Boltzmann constant, $B = (\varepsilon_{\mathrm{AA}}/k)^{1/2}T^{-1}$, $\varepsilon_{\mathrm{AA}}$ is the potential well depth of the dimer A_2, T is the temperature. The Boltzmann average broadening widths in Table 1 were converted to Boltzmann weighted collision cross sections of OH with foreign gases by first converting them into SI units (Hz Pa^{-1}) and then multiplying by the factor $\pi k T \upsilon_0^{-1}$, where k is the Boltzmann's constant, T is the gas temperature in K and υ_0 is the mean relative velocity of the colliding pair [14]. The collision cross sections in Å^2 were computed to be 87 ± 13, 63 ± 9, 34 ± 8 and 19 ± 7 for N_2, Ar, Ne and He, respectively. The PS plot is shown in Figure 3 with the dimer well depths taken from [13]. The experimental points for He, Ne and Ar points were fitted with a straight line with a correlation coefficient of 0.995 and constants A and B were estimated to be 2.37 ± 0.1 and 0.17 ± 0.01 by the least squares method. Our experimental $(\varepsilon_{\mathrm{OH(X)-OH(X)}}/k)^{1/2}$ value of 52 ± 4 K^{-1} is close to values of 54 ± 5 K^{-1} [7] and 61 ± 10 K^{-1} [8] derived from the experimental pressure broadening widths of absorption A $^2\Sigma^+$ ($\upsilon' = 0$) $\leftarrow$ X $^2\Pi_{3/2}$ ($\upsilon'' = 0$) transitions measured at 293 K and 296 K, respectively.

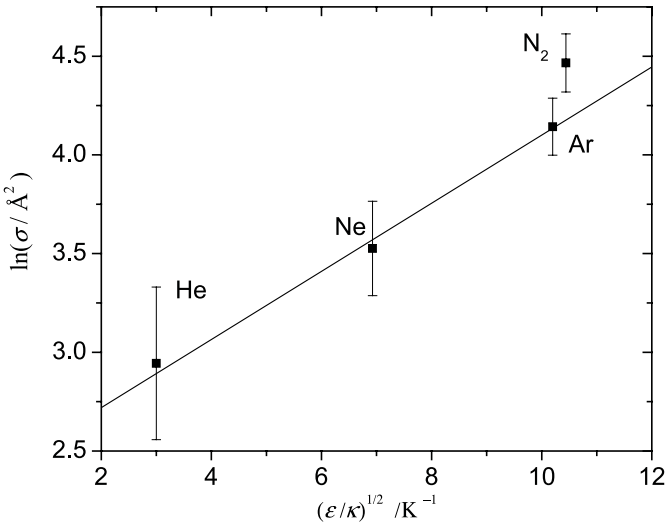

Fig. 3. The Parmenter-Seaver plot for the pressure broadening of hydroxyl radical. The parameter σ is the Boltzmann averaged collision cross-section calculated from the experimental pressure broadening width for OH in N_2, Ar, Ne and He. The parameter ε is the potential well depth of the dimer of the colliding partner.

In our experiments it was not possible to observe OH absorption in wet molecular oxygen flow at atmospheric pressure because of fast removal of OH by oxygen atoms formed in the sample cell through a vacuum UV photolysis of molecular oxygen. We used the PS relationship to estimate the OH Boltzmann average pressure broadening width in O_2. For oxygen $(\varepsilon_{\mathrm{O_2-O_2}}/k)^{1/2} = 10.677$ K^{-1} [12], we find from the PS plot data that the OH collision cross section in oxygen is 68 ± 11 Å^2. Hence, the OH pressure broadening full width induced by O_2 is 4.0 ± 0.7 GHz atm^{-1}. Our estimation of the OH collisional width for oxygen is comparable with 3.8 GHz atm^{-1} averaged over A $^2\Sigma^+$ ($\upsilon' = 0$) $\leftarrow$ X $^2\Pi_{3/2}$ ($\upsilon'' = 0$) lines [7] and 4.3 ± 0.2 GHz atm^{-1} measured for $P_{11}(1)$ transition [8] but lower than 5.2 ± 0.3 GHz atm^{-1} [5].

Finally, we calculate the OH average pressure broadening width by air (79% N_2 and 21% O_2) as 5.0 ± 0.6 GHz atm^{-1} which is close to values of 5.82 GHz atm^{-1} and 5.16 GHz atm^{-1}derived from pressure broadening measurements of rotational OH transitions with $N'' = 1, 2$ and used in the HITRAN database at a temperature of 296 K [6].

The pressure-induced frequency shift x_c is dependent on the imaginary component of the collision cross section and is typically represented as a fraction of the collisional width w_c as $x_c = \beta w_c$ [15]. From the plot of the pressure-induced shift against pressure broadening width for Ar, Ne and He we have estimated the coefficient $\beta = -0.15$ with a correlation coefficient of -0.87. This value is similar to the pressure-induced shift $\beta = -0.11$ measured for OH P_{11} (6.5) transition of A $^2\Sigma^+$ ($v' = 1$) $\leftarrow$ X $^2\Pi_{3/2}$ ($v'' = 0$) band at ca. 283 nm.

We briefly consider the implication of our measurements for the OH detection at diurnal concentrations of $1{-}10 \times 10^6$ molecule cm^{-3} observed in the atmosphere [4]. We calculate that for the OH Doppler broadening linewidth of 2.9 GHz a peak absorption cross section of $Q_{11}(2)$ transition is 6.2×10^{-16} cm^2 molecule^{-1} at a low pressure of $\sim$1 Torr. Thus, in the case of the direct absorption sensitivity of 5×10^{-5} Hz$^{-1/2}$ a detection limit of 10^6 molecule cm^{-3} in a time of 10 s can be reached at total absorption cell pathlength of 255 m. This path length can be achieved in an optical cell based on Herriott design [16].

5 Conclusions

Absorption spectroscopy of the hydroxyl radical in the UV spectral region was performed at low pressure and atmospheric pressure using sum-frequency generation of two diode lasers with the wavelengths of $\sim$488 nm and $\sim$835 nm. A bandwidth-normalised noise equivalent absorption of 5×10^{-5} Hz$^{-1/2}$ was demonstrated in the case of direct absorption measurements of the OH radicals at atmospheric pressure. Pressure broadening parameters for four of the OH strongest lines in the A $^2\Sigma^+$ ($v' = 0$) $\leftarrow$ X $^2\Pi_{3/2}$ ($v'' = 0$) band at ca. 308 nm have been determined for N_2, Ar, Ne and He. The OH pressure broadening average width of 4 ± 0.7 GHz atm^{-1} by O_2 was estimated using a Parmenter-Seaver intermolecular potential well depth correlation.

The work has been funded by the NERC under the COSMAS program.

References

1. J. Franzke, R.W. Fox, L. Hollberg, Spectrochim. Acta B. **53**, 1951 (1998)
2. J. Alnis, U. Gustafsson, G. Somesfalean, S. Svanberg, Appl. Phys. Lett. **76**, 1234 (2000)
3. T. Laurila, R. Hernberg, Appl. Phys. Lett. **83**, 845 (2003)
4. D.E. Heard, M.J. Pilling, Chem. Rev. **103**, 5163 (2003)
5. H.P. Dorn, R. Neuroth, A. Hofzumahaus, J. Geophys. Res. **100**, 7397 (1995)
6. J.R. Gillis, A. Goldman, G. Stark, C.P. Rinsland, J. Quant. Spectrosc. Radiat. Transf. **68**, 225 (2001)
7. R. Engleman, J. Quant. Spectrosc. Radiat. Transfer. **9**, 391 (1969)
8. B. Shirinzadeh, D.M. Bakalyar, C.C. Wang, J. Chem. Phys. **82**, 2877 (1985)
9. G. Hancock, V.L. Kasyutich, Appl. Phys. B **79**, 383 (2004)
10. J. Luque, D.R. Crosley, "LIFBASE: Database and spectral simulation (version 1.5)", SRI International Report MP 99-009 (1999)
11. E.E. Whiting, J. Quant. Spectrosc. Radiat. Transf. **8**, 1379 (1968)
12. D.E. Heard, D.A. Henderson, Phys. Chem. Chem. Phys. **2**, 67 (2000)
13. C.S. Parmenter, M. Seaver, J. Chem. Phys. **70**, 5458 (1979)
14. D. Bastard, A. Bretenoux, A. Charru, F. Picherit, J. Quant. Spectrosc. Radiat. Transf. **21**, 369 (1979)
15. W.J. Kessler, M.G. Allen, S.J. Davis, J. Quant. Spectrosc. Radiat. Transf. **49**, 107 (1993)
16. D. Herriott, H. Kogelnik, R. Kompfner, Appl. Opt. **3**, 523 (1964)